Supplementary Materials

Tellurite Anti-Resonant Hollow-Core Fiber: Fabrication, Mid-Infrared Femtosecond Laser Transmission, and Application in Tissue Ablation

Jun Zhu†, Chengzhen Liu†, Ang Deng†, Ziqian Zhang, Yanjie Chang, Hao Zhang, Yantao Xu, Xusheng Xiao, Yang Xiao, Zhizhuo Fu, Dunxiang Zhang, Chaoqi Hou, Houkun Liang*, Yuxi Fu*, and Haitao Guo*

This file includes:

Other Supplementary Materials for this manuscript include the following:

Supplementary Text

Basic thermal stability and optical transmission of tellurite glass.

Compared to silica or chalcogenide glasses, tellurite glass exhibits lower thermal stability, complicating its reuse in multiple drawing operations due to crystal formation. This study proposes a tellurite glass component that exhibits exceptional thermal stability, as shown by its differential scanning calorimetric curve in Fig. S1 (A). The glass transition temperature (Tg) and the onset of precipitation temperature (T_x) for this component are 419.8 ℃ and 561.5 ° C, respectively. The value of $\Delta T=T_g-T_x$, which measures the thermal stability, is 141.7 °C, which allows for the multiple pulling process of the AR-HCF. As illustrated in Fig. S1 (B), the transmission curve of 3 mm thick tellurite bulk glass ranges from 300 to 7000 nm. Through a series of purification processes, the hydroxyl absorption coefficient was reduced to 0.025 cm^{-1}. Hydroxyl absorption in the material has minimal impact on the laser transmission of the tellurite AR-HCF.

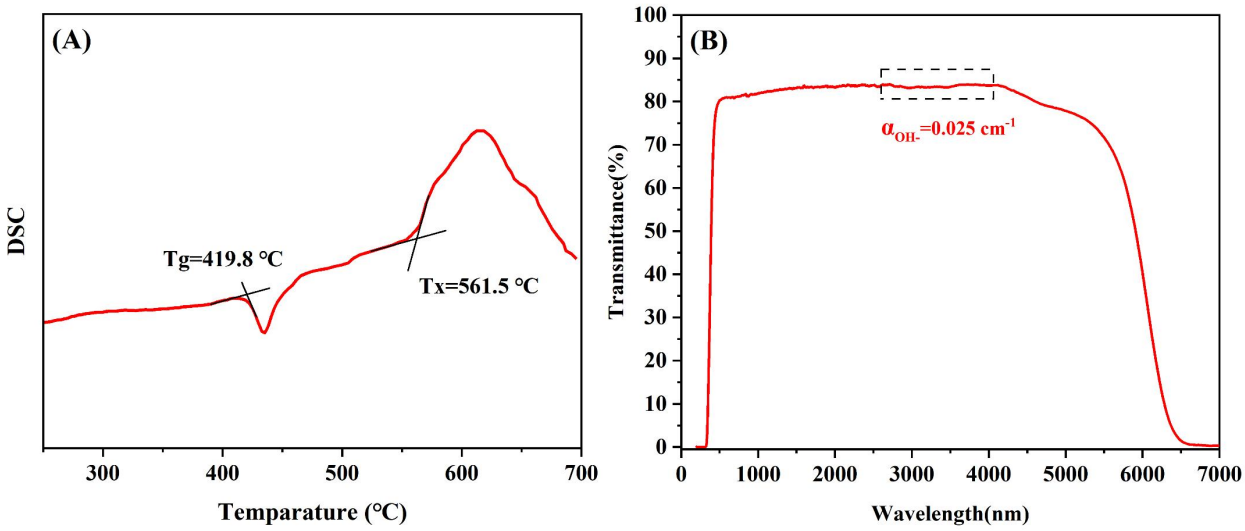

Fig. S1.

(A) DSC curve of tellurite glass. (B) Transmission in 300–7000 nm of tellurite glass with a thickness of 3 mm.

Supplementary Text

Loss simulation of silica AR-HCF.

Here, based on similar structural design and simulation approaches, we simulated the theoretical loss of silica AR-HCF. Figs. S2 (a) and (b) show the bulk material loss and refractive index of quartz glass, respectively. Fig. S2(c) compares the theoretical loss of AR-HCF made from both materials across different wavelengths. Silica AR-HCF exhibits losses exceeding 1 dB/m at wavelengths above 5 μm, whereas tellurite AR-HCF reaches 1 dB/m at 10 μm. Simulation results demonstrate that tellurite AR-HCF exhibits superior transmission capabilities in the mid-infrared band compared to silica AR-HCF.

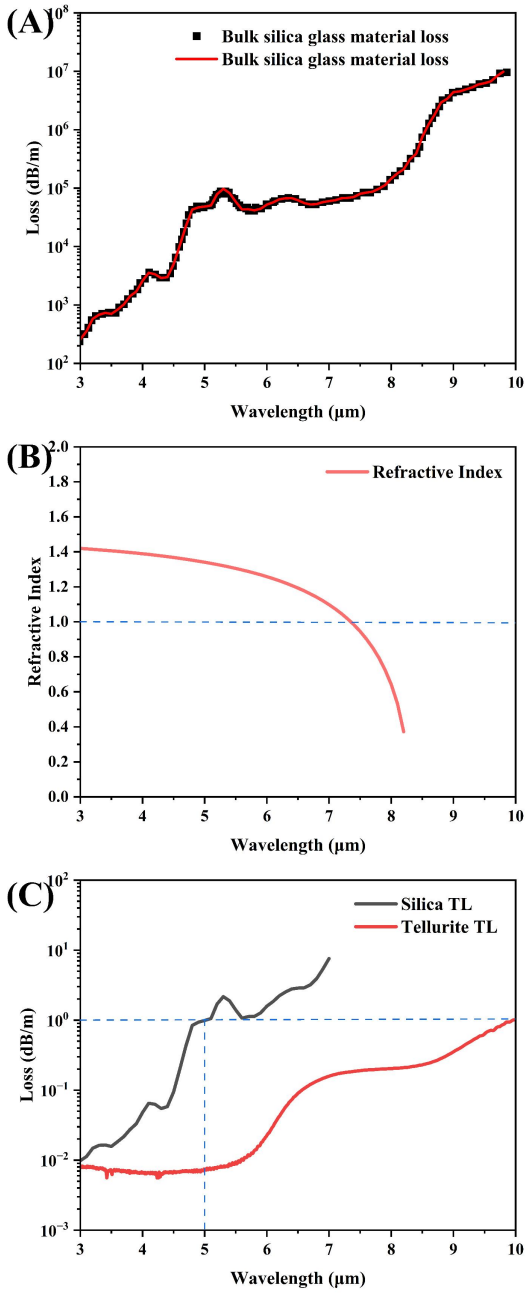

Fig. S2.

(A) Bulk silica glass material loss; (B) Refractive index of silica glass; (C) Comparison of theoretical total loss between silica AR-HCF and tellurite AR-HCF under identical structural design methods.

Supplementary Text

Long-duration laser tolerance of tellurite AR-HCF.

Additionally, the power stability of a 5.75 μm femtosecond laser transmitted through Fiber A was assessed over different durations. The fiber length was 40 cm, with an input power set at 80 mW and an output power of 40 mW achieved. Fig. S3 (A) shows the morphology of the fiber's incident end after 60 minutes of uninterrupted transmission, indicating that the laser did not cause any loss of fiber functionality. Fig. S3 (B) displays the variation of fiber output power over time, with a measured root mean square (RMS) of 0.616%, indicating that the tellurite AR-HCF can operate for extended periods during laser transmission.

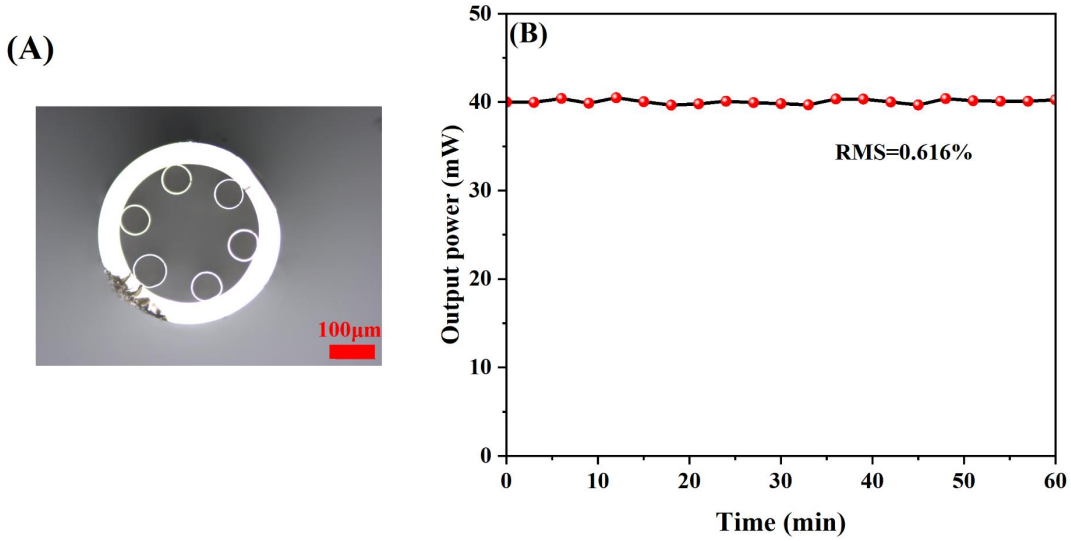

Fig. S3.

(A) Fiber cross-section at the incident end of tellurite AR-HCF after transmitting 5.75 μm laser for 60 min. (B) Stability of the output laser in a 60 min output at 40 mW.

Supplementary Text

Anti-resonance transmittance characteristics of tellurite AR-HCFs with different capillary wall thicknesses in the 3–11 μm range.

Fig. S4 displays the output normalized spectral intensities of telluride AR-HCF with three different wall thicknesses t (2.9, 3.3, and 4.3 μm), using a Fourier Transform Infrared (FTIR) spectrometer as the laser source. Due to the difficulty of transmitting laser light above 3.5 μm in telluride solid-core fibers of a given length, the spectral intensities obtained in the tests can be attributed to core transmission rather than glass transmission. The correspondence between spectral intensity and wall thickness is evident, with each of the first-order (I_{AR}), second-order (II_{AR}), and third-order (III_{AR}) anti-resonance bands corresponding to a specific wall thickness. First-order markers are red, second-order markers are orange, third-order markers are blue, and fourth-order markers are violet. As the wall thickness increases, the antiresonance transmission band shifts toward the long-wave direction. Additionally, the first-order transmission band with a thickness of 3.3 μm clearly exceeds 10 μm, reaching nearly 11 μm, demonstrating that the laser transmission window of the tellurite AR-HCF is significantly wider than that of the silica AR-HCF.

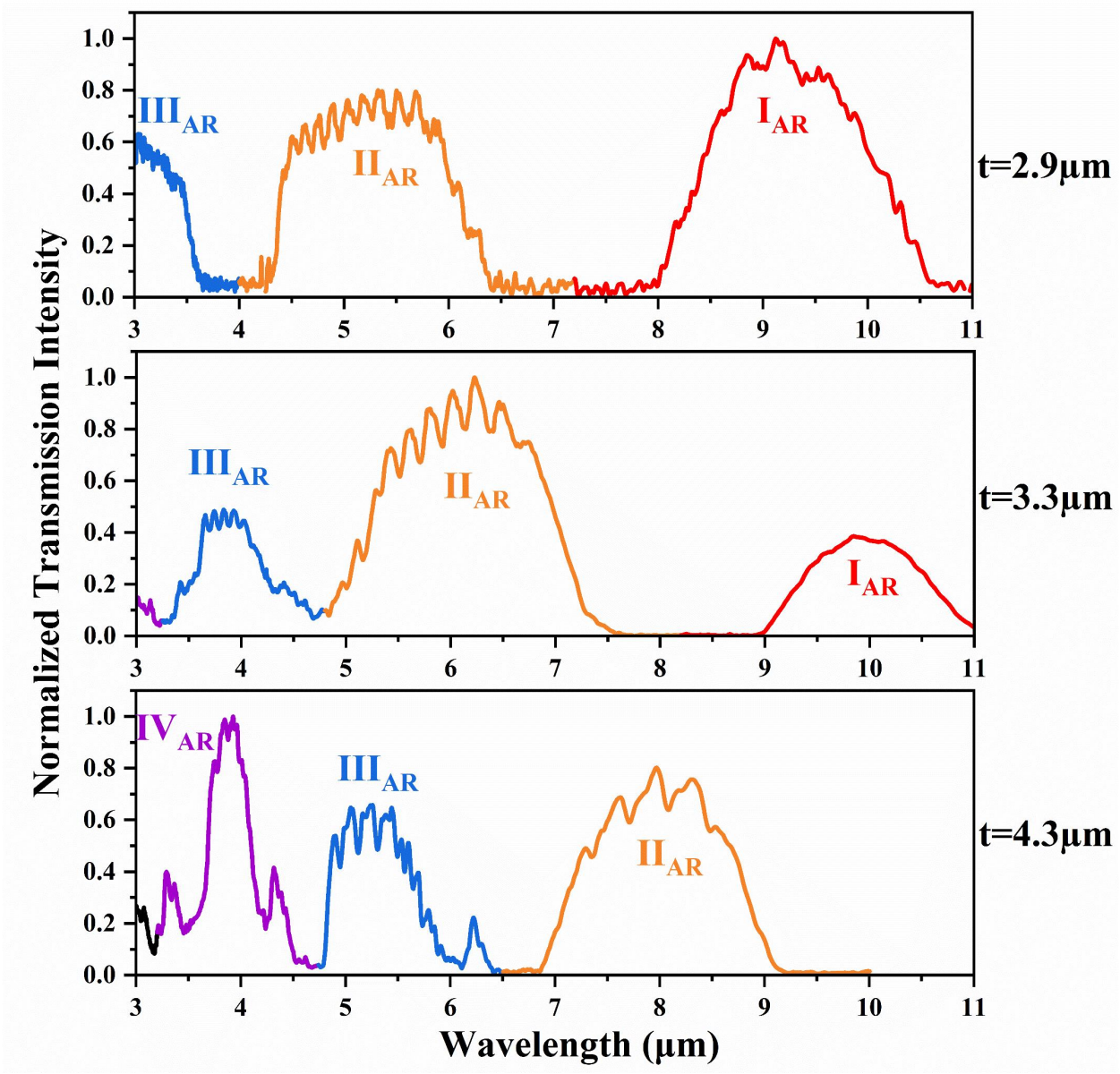

Fig. S4.

Normalized transmission spectral intensities of tellurite AR-HCFs transmission FTIR spectrometer sources with capillary wall thicknesses of 2.9 μm, 3.3 μm and 4.3 μm.

Supplementary Text

Porcine liver cutting experiment.

In addition, a 6.1 μm femtosecond laser transmitted by a tellurite anti-resonant hollow-core fiber was used to perform cutting experiments on porcine liver tissue, as shown in Fig. S5. The cutting effect was achieved with an average fiber output power of 40 mW, which was attributed to the optimization of the fiber for laser quality.

Fig. S5.
Cutting of porcine liver using a tellurite AR-HCF transmitting a 6.1-μm femtosecond laser

Supplementary Text

Experimental setup on femtosecond laser ablation of biological tissues by tellurite AR-HCF transmission.

The femtosecond laser is generated by an OPA system and focused by a lens into a tellurite AR-HCF. The femtosecond laser output from the fiber was not collimated and focused, but was directly subjected to tissue ablation experiments.

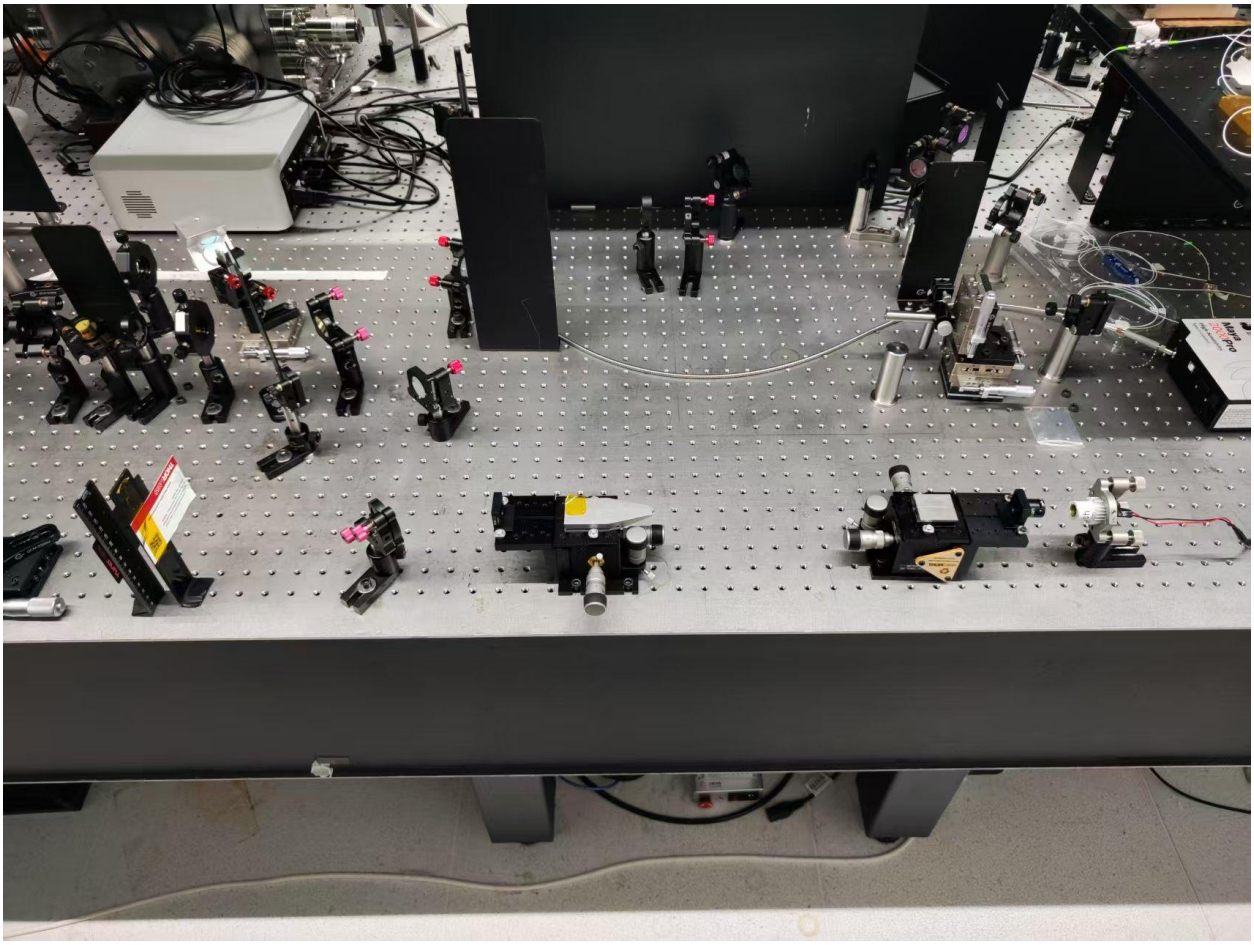

Fig. S6.
Experimental setup of ultrafast laser transmission through tellurite AR-HCF

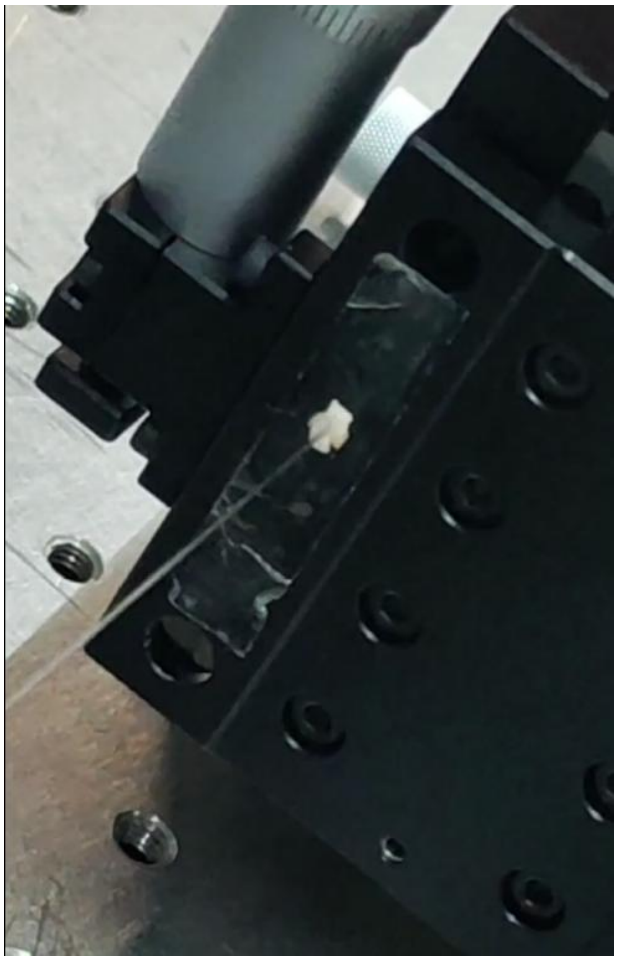

Movie S1.
Femtosecond laser ablation of biological tissues by tellurite AR-HCF transmission